# Light ion vertex form factors using realistic overlap functions

A. M. Eiró
*Departamento de Física and Centro de Física Nuclear, Universidade de Lisboa, 1700 Lisboa, Portugal*

I. J. Thompson
*Department of Physics, University of Surrey, Guildford GU2 5XH, United Kingdom*
(Received 16 October 1998)

To test the model dependence of the extracted asymptotic parameters, we reanalyze published $(d,t)$, $(d,^3\mathrm{He})$ $(d,\alpha)$, and $(d,^6\mathrm{Li})$ reactions, comparing recent variational Monte Carlo (VMC) microscopic vertex form factors with those used previously. In the $(d,t)$ reactions studied the tensor observables are found to be proportional to $\eta$, in $(d,^3\mathrm{He})$ and $(d,\alpha)$ transfers there is some sensitivity to the vertex shape, while for $(d,^6\mathrm{Li})$ there is a strong shape dependence. Comparisons with data show that the $D$ states in the three- and four-body VMC vertex functions are slightly too weak. In the $(d,^6\mathrm{Li})$ reaction the polarization data are not reproduced, clearly indicating that the $D$-state components of the new $^6$Li models are too strong.
[S0556-2813(99)06605-4]

PACS number(s): 24.70.+s, 24.10.Eq, 25.10.+s, 25.45.Hi

## INTRODUCTION

Transfer reactions have been extensively used to investigate the internal structure of nuclei. In particular the measurement of polarization observables in reactions induced by light ions has shown to be particularly adequate for the determination of structure parameters of light projectiles [1].

In a stripping reaction of $A(a,b)B$ type, where $a=b+x$, the form factor involved is

$$\langle Bb|V_{bx}|aA\rangle=\langle B|A\rangle\langle b|V_{bx}|a\rangle, \tag{1}$$

where the light ion vertex form factor can be written as

$$V\psi\equiv\langle b|V_{bx}|a\rangle=-(B_{ab}+T)\langle b|a\rangle. \tag{2}$$

This vertex form factor $V\psi$ is a function of $r$, contains all the dependence on the internal structure of the light nucleus, and has been summarized by its volume integral, the vertex constant.

The method most frequently used in finite-range transfer analyses is a separation energy procedure, where the different angular momentum components of the $\langle b|a\rangle$ overlaps are generated in potential wells, generally of Woods-Saxon shape, chosen to reproduce ''known'' radii and vertex constants. This approximate finite-range procedure has the advantage of imposing a correct asymptotic behavior on the different components of the wave function, which is a determining feature for reactions which occur in the peripheral region. Preferably, however, one should use realistic wave functions for the $a$ and $b$ systems. Recently Forest *et al.* [2] obtained, in a variational Monte Carlo (VMC) calculation, the overlaps functions for a series of light particles using the new realistic two nucleon interaction Argonne v18 and the Urbana model IX three nucleon interaction [3]. We also consider more recent VMC calculations [4] which are apparently more close to convergence.

To test the model dependence of transfer reactions to the use of these realistic overlaps, we reanalyze in this paper several published $(d,t)$ [5], $(d,^3\mathrm{He})$ [6], $(d,\alpha)$ [7], and $(d,^6\mathrm{Li})$ [8,9] reactions. In our present analysis we therefore keep the optical potentials found previously in the literature to best describe the entrance and exit channels, and keep the same target bound state wave functions for the transfers, but substitute for the projectile vertex form factors the results from the VMC calculations. In each reaction we check the proportionality of the calculated analyzing powers to the asymptotic parameters, and the sensitivity to the detailed shape of the vertex functions. Comparisons with data then allow us to make some conclusions about whether or not it is useful to use the VMC wave functions.

## REALISTIC VERTEX FORM FACTORS

The VMC results of Forest *et al.* [2,4] are presented in terms of the overlap wave function in momentum space. Ideally, the vertex functions $V\psi$ would be found directly by substitution in Eq. (2), the one-channel Schrödinger equation. However, this requires second derivatives of the overlap functions to get the different components of the vertex functions, and the results always exhibit some oscillations and nonexponential decays in their tails, whichever $q_{\max}$ we choose for the upper limit of the momentum distributions.

We found more consistent results with an improved method, of fitting the momentum distributions of Forest *et al.* [2,4] to a Fourier transform of a linear combination of interior and exterior basis wave functions each of which exhibits a good behavior at $r=0$ or $r=\infty$, respectively. For large distances, in particular, we force the wave function to have the correct asymptotic decay as given by the experimental separation energy $B_{ab}$. (The VMC energies are themselves too inaccurate to be used directly at this point.) We use, therefore, for each angular momentum component $l=0$ and 2, polynomials of the type $\Sigma_{n=l}a_n r^n$ for $r<R_0$, and $\Sigma_{n=0}b_n/r^{n+1}W_{-\eta_c,l+1/2}(2\kappa r)$ for $r>R_0$, where the Whittacker functions $W_{-\eta_c,l+1/2}$ are calculated for bound state wave numbers $\kappa$, corresponding to the experimental binding energies. The parameters $a_n$ and $b_n$ are determined by the

 

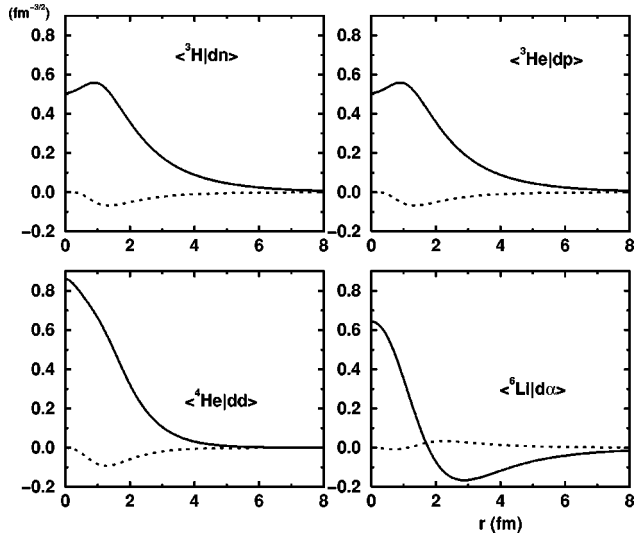


FIG. 1. Radial wave functions for the fitted $l=0$ components of $\langle {}^3\mathrm{H}|dn\rangle$, $\langle {}^3\mathrm{He}|dp\rangle$, $\langle {}^4\mathrm{He}|dd\rangle$, and $\langle {}^6\mathrm{Li}|d\alpha\rangle$ as the full curves, and the $l=2$ components as the dotted curves.

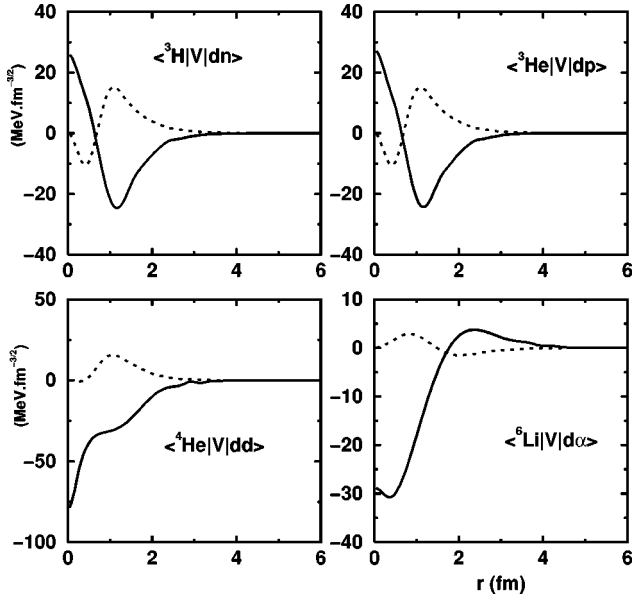


FIG. 2. Radial vertex functions for the fitted $l=0$ components of $\langle {}^3\mathrm{H}|V_{dn}|dn\rangle$, $\langle {}^3\mathrm{He}|V_{dp}|dp\rangle$, $\langle {}^4\mathrm{He}|V_{dd}|dd\rangle$, and $\langle {}^6\mathrm{Li}|V_{d\alpha}|d\alpha\rangle$ as the full curves, and the $l=2$ components as the dotted curves.

minimum of a $\chi^2$ fit (the data of Ref. [2] has statistical errors for each $q$ value), and $R_0$ was set to 2 fm. This value was chosen to minimize the number of parameters needed in the fit. We used five parameters to describe the $l=0$ $S$-wave function and five for the $l=2$ $D$ channel, but there is little change if more are included. The results of these fits are given in Figs. 1 and 2, where we show as functions of radius $r$ in fm the $l=0$ components of $\psi$ (Fig. 1) and $V\psi$ (Fig. 2) for the four cases $\langle t|nd\rangle$, $\langle {}^3\mathrm{He}|pd\rangle$, $\langle {}^4\mathrm{He}|dd\rangle$, and $\langle {}^6\mathrm{Li}|d\alpha\rangle$ as the full curves, and the $l=2$ components as the dashed curves.

We now perform a series of calculations using our fitted vertex functions, to enable comparisons with a range of recent experiments. For the $(d,t)$ reactions we examine the recently measured [5] transfer processes $^{119}\mathrm{Sn}(d,t)^{118}\mathrm{Sn}(1/2^+)$ at $E_d=5.25$ MeV, $^{149}\mathrm{Sm}(d,t)^{148}\mathrm{Sm}(7/2^-)$ at $E_d=6$ MeV, and $^{206}\mathrm{Pb}(d,t)^{205}\mathrm{Pb}(3/2^-)$ at $E_d=10$ MeV. For the $(d,{}^3\mathrm{He})$ reaction we analyze the $^{93}\mathrm{Nb}(d,{}^3\mathrm{He})^{92}\mathrm{Zr}(9/2^+)$ transfer process at $E_d=12$ MeV [6]. For the $(d,\alpha)$ reaction we considered $^{58}\mathrm{Ni}(d,\alpha)^{56}\mathrm{Co}(7^+)$ at $E_d=22$ MeV [7], and finally for the $(d,{}^6\mathrm{Li})$ overlap process we look at the inverse $^{58}\mathrm{Ni}({}^6\mathrm{Li},d)^{62}\mathrm{Zn}(0^+)$ transfer cross section at $E_{\mathrm{Li}}=34$ MeV [8,9].

Because of the tensor observables measured in the reactions we will consider, our analysis will probe mainly the description of the $l=2$ components. We compare in Table I the $D$-state parameters of the VMC wave functions from Refs. [2,4] with the latest values extracted from experiments. We also show the parameters calculated with the fitted wave function obtained as described above, and in the final columns to the best experimental values. In the table we present two measures of the $D$-state contributions $D_2$ and $\eta$. The first is defined by

$$D_2=\lim_{k\to 0}\frac{\phi_2(k)}{k^2\phi_0(k)}=\frac{\int_0^\infty \psi_2(r)r^4dr}{15\int_0^\infty \psi_0(r)r^2dr}, \tag{3}$$

where $\phi_l(k)=\int_0^\infty j_l(kr)\psi_l(r)r^2dr$ are the momentum-space wave functions. The $\eta=N_2/N_0$, is the ratio of the asymptotic normalization coefficients, with $N_l$ defined by $\psi_l(r)\to_{r\to\infty}N_l W_{-\eta_c,l+1/2}(2\kappa r)/r$ for bound state wave numbers $\kappa$ and Whittaker function $W_{-\eta_c,l+1/2}$.

It is also of interest to examine the $S$-state vertex functions, and the relative $S$- and $D$-state probabilities, and com-

TABLE I. Comparison of original and fitted VMC predictions with experimental results from [1] (unless otherwise indicated).

| | VMC results from Ref. [2] | | Fitted VMC results | | Experiment | |
|---|---|---|---|---|---|---|
| Overlap Function | $D_2$ (fm$^2$) | $\eta$ | $D_2$ (fm$^2$) | $\eta$ | $D_2$ (fm$^2$) | $\eta$ |
| $(d,t)$ | $-0.15(1)$ | $-0.037$ | $-0.17$ | $-0.037(3)$ | $-0.23(5)$ | $-0.041(1)$ [5] |
| $(d,{}^3\mathrm{He})$ [2] | $-0.15(1)$ | $-0.035$ | $-0.18$ | $-0.035(3)$ | $-0.25(4)$ | $-0.039(1)$ [6] |
| $(d,\alpha)$ [2] | $-0.12(1)$ | $-0.091$ | $-0.10$ | $-0.095(10)$ | $-0.19(4)$ | |
| $(d,{}^6\mathrm{Li})$ [2] | $-0.29(1)$ | $-0.07(2)$ | $-0.53$ | $-0.05(2)$ | | $+0.0003(9)$ [9] |
| $(d,{}^6\mathrm{Li})$ [4] | | | $-0.37$ | $-0.03(1)$ | | |

TABLE II. Normalizations of the $S$- and $D$-wave VMC overlaps, and their vertex constants $D_0$ and $D$. The WS columns show the adopted Woods-Saxon normalizations, and then the vertex constants from such wave functions.

| Model transfer reaction | VMC wave functions $C^2S$ $S$ wave | $C^2S$ $D$ wave | $D_0$ (MeV fm$^{3/2}$) | $D$ (MeV fm$^{3/2}$) | WS approximations $C^2S$ $S$ wave | $D_0$ (MeV fm$^{3/2}$) | $D$ (MeV fm$^{3/2}$) |
|---|---|---|---|---|---|---|---|
| $(d,^3\mathrm{H})$ | 1.31 | 0.022 | $-204$ | $-230$ | 2 | $-165$ | $-182$ |
| $(d,^3\mathrm{He})$ | 1.31 | 0.022 | $-182$ | $-193$ | 2 | $-151$ | $-155$ |
| $(d,\alpha)$ | 0.98 | 0.024 | $-320$ | $\sim -620$ | 2 | $-282$ | $-458$ |
| $(d,^6\mathrm{Li})$ [2] | 0.82 | 0.021 | $-67$ | $\sim -82$ | 1 | $-68$ | $-66$ |
| $(d,^6\mathrm{Li})$ [4] | 0.85 | 0.016 | $-65$ | $\sim -78$ | 1 | $-68$ | $-66$ |

pare the VMC predictions with those of simpler approximations which have been widely used in the past. In each reaction, we therefore compare the transfer cross sections and analyzing powers with the results using a Woods-Saxon binding potential. The projectile binding potentials all have diffuseness $a=0.50$ fm, and radius $R=1.5$ fm for the case of $(d,t)$ and $(d,^3\mathrm{He})$ and $R=1.9$ fm for the $(d,\alpha)$ and $(^6\mathrm{Li},d)$. We compare in Table II the parameters obtained of our fitted VMC wave functions with these more common WS approximations. The $C^2S$ are the normalizations of the VMC fractional overlap functions. Since the WS wave functions are normalized to unity, they need to be multiplied by the corresponding normalizing amplitude $(C^2S)^{1/2}$. In Table II, the parameter $D_0$ is the usual [10] zero-range constant

$$D_0 = -B_{ab}\sqrt{4\pi}\int \psi_0(r)r^2dr = \sqrt{4\pi}\int (V\psi)_0(r)r^2dr \tag{4}$$

calculated from either the overlap wave function or the vertex function. By $(V\psi)_0(r)$ we refer to the sum of the contributions from the $S$ and $D$ waves: $(V\psi)_0(r)=V_{00}(r)\psi_0(r)+V_{02}(r)\psi_2(r)$. For sub-Coulomb reactions in the local energy approximation, the cross section is proportional to the square not of $D_0$ but of $D\equiv D_0(1+\kappa^2 r_e^2)$, where $r_e$ is the so-called ''effective range.'' This $D$ is the residue of the vertex function $D(q)$ at the pole $q=i\kappa$. In the zero range approximation, where $V_{bx}$ is represented by a $\delta$-function interaction and the normalized wave function is given by its asymptotic form, the parameters $D$ and $D_0$ are equal and given by

$$D=\frac{\sqrt{4\pi}\hbar^2}{2\mu}N_0 \tag{5}$$

showing a direct connection with the tail normalization $N_0$ of the projectile overlap wave function $\psi_0(r)$. In the local energy approximation, $D$ becomes the zero-range constant appropriate for sub-barrier transfers, and differs from $D_0$ because of the potentials having finite range. We give the $D$ parameter in Table II as another measure of the long-range tail of the projectile overlap.

The magnitudes of the transfer cross sections are expected (e.g., according to the zero range approximation) to be proportional to $D_0^2$ for the VMC case, but to $C^2S\times D_0^2$ for the WS wave functions since these are normalized to unity. The WS and VMC results in Table II give therefore roughly similar magnitudes (some differences in magnitudes will become apparent), but the analyzing powers should depend only on the ratios of the cross sections, and are therefore independent of normalizations. All of the calculations below use full finite range form factors in FRESCO [11] in a one-step approximation. The $D$-wave WS wave functions are found in potentials of the above shapes, and transfer calculations are performed with the $D/S$ amplitudes chosen to give either the $\eta$ value for the best fit to the experiments, or the $\eta$ value estimated from the VMC models.

## RESULTS AND DISCUSSION

We now reanalyze some published light-ion transfer reactions to examine the sensitivity to the treatment of the projectile vertex. We therefore keep the optical potentials found previously in the literature to best describe the entrance and exit channels, the same target bound state wave functions for the transfers, and merely substitute for the previous projectile vertex form factors the results of the VMC calculations. From the existing comprehensive surveys of experimental evidence for each projectile, we choose in each reaction a ''typical'' target final state. There are in the literature uncertainties concerning potentials and target wave functions, but these questions can not be reexamined here if we wish to isolate the effect of the projectile vertex. The published reactions are sub-Coulomb where possible to minimize the effects of optical potentials, and usually use target states chosen to minimize configuration mixing.

The first transfer reaction we consider is that of $(d,t)$ one-neutron transfers at energies that are well below the barrier. Much experimental effort has been devoted to measuring accurately the tensor analyzing powers of such reactions, since they afford a clean probe of the triton $D$ state. If pure angular momentum transfers for the targets are selected by a good choice of final states, then the tensor analyzing powers are almost entirely just proportional to the projectile $D$-state components. The $(d,t)$ reaction, moreover, allows both the initial and final channels to be entirely in the sub-Coulomb regime, and hence it is possible to minimize the effects of the nuclear potentials in both the entrance and exit channels. The deuteron tensor force, in particular, has only a very weak contribution to the tensor analyzing powers. We consider three reactions to specific final states $^{119}\mathrm{Sn}(d,t)^{118}\mathrm{Sn}(1/2^+)$ at $E_d=5.25$ MeV, $^{149}\mathrm{Sm}(d,t)^{148}\mathrm{Sm}(7/2^-)$ at $E_d=6$ MeV, and $^{206}\mathrm{Pb}(d,t)^{205}\mathrm{Pb}(3/2^-)$ at $E_d=10$ MeV. The data for these reactions are from Ref. [5], and are shown in Fig. 3.

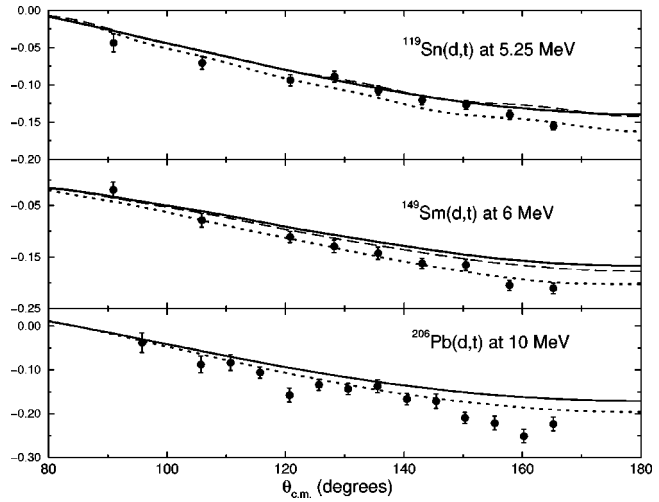


FIG. 3. Tensor observables $A_{zz}$ for the $(d,t)$ transfer reactions with the targets and energies indicated. The solid line gives the VMC predictions ($\eta=-0.037$), the dotted line the WS best fit to the data ($\eta=-0.041$), and the dashed line the WS wave functions adjusted to the VMC $\eta$ value.

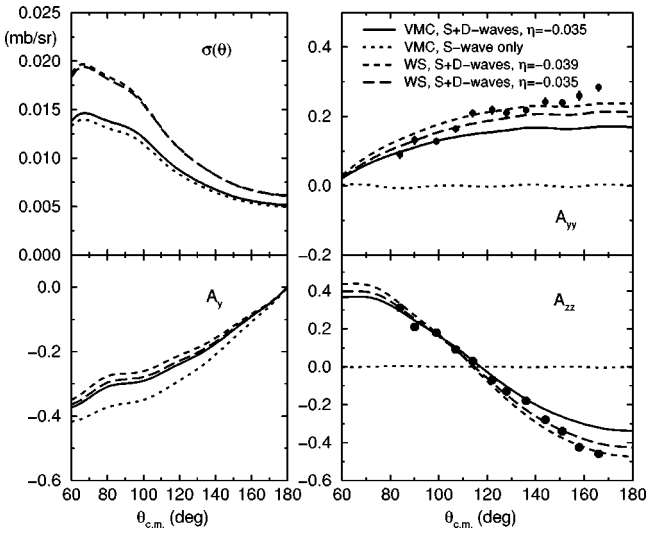


FIG. 4. $^{93}$Nb$(d,^3$He$)^{92}$Zr$(9/2^+)$ at $E_d=12$ MeV. The VMC curves use the revised results of Ref. [2], and the WS $D$-state curves use the $\eta$ $D$-state amplitudes indicated.

The dotted curve gives from [5] the best fit to the data with WS projectile binding potentials, while the solid curves are the direct consequence of the VMC vertex functions. We see that the $\eta$ value from the VMC calculations is consistently 10% smaller in absolute value than that needed to fit the experimental data. In these good sub-Coulomb reactions, where only the overlap tails are significant, we find (by the dashed line) that the VMC results are well approximated by WS form factors adjusted to have the same $\eta$ values. This indicates that the description of the data is rather strictly proportional to the $\eta$ value, and that the failure of the VMC can be directly traced to the small $\eta$ value calculated already in Ref. [2] and seen again in Table I.

The second transfer reaction considered is a one-proton $(d,^3$He) transfer reaction. Ideally, this should yield results of similar accuracy to the $(d,t)$ transfer experiments, but in practice there is found to be considerably more sensitivity to the optical potentials. This is because the experiments cannot be performed at an energy that is sub-Coulomb in both entrance and exit channels, due to the change in the projectile charge. Nevertheless, we can consider a typical $(d,^3$He) reaction from Ref. [6]: the $^{93}$Nb$(d,^3$He$)^{92}$Zr$(9/2^+)$ transfer process at $E_d=12$ MeV. The data for this reaction are shown in Fig. 4, from Ref. [6]. Again, the projectile $S$ states only allow pure $L$ transfers to the chosen final state, so all the $A_{yy}$ and $A_{zz}$ tensor analyzing powers are seen to arise from the projectile $D$ state. Model calculations show that these tensor observables scale with the $\eta$ values of the $(d,^3$He) vertex, but in Fig. 4 we see that VMC and WS calculations that both use $\eta=-0.035$ (the solid and long dashed lines, respectively) give somewhat different results. This means that the $(d,^3$He) reaction is not purely sensitive to $\eta$ for the tail of the overlap function, but depends also on interior properties. The predictions of $\sigma(\theta)$ have different overall normalizations as mentioned previously, leading to $\sigma_{\rm WS}(\theta)>\sigma_{\rm VMC}(\theta)$ as expected from the comparison of the zero range constants in Table I, but the tensor observables will not be directly affected by this. We see that the values of $\eta$ differ by 11% (see Table I), and that again the VMC models underestimate the asymptotic $D$-state amplitudes. Moreover, in view of the different predictions obtained form WS and VMC models for the same $\eta$, this underestimation is likely to be stronger, up to approximately 25%, since the shape of the VMC $D$-state overlap differs from that of the WS model.

The $\alpha$-particle is very tightly bound and spherical, but still allows, on being separated into two deuterons, for the deuterons to have both $S$ and $D$ states of relative motion. The magnitude of this $D$-wave component has not been easy to determine using $(d,\alpha)$ reactions, because the transferred $n+p$ pair has spin 1. Even for well chosen reactions (induced on $0^+$ targets and therefore having a well defined $J$ transfer), the only transfers with unique $L$ are the natural parity transitions, which are the ones where $D$-state effects are smaller [1]. In all the other transitions, the unnatural parity ones, there is a mixing of $L$ transfer, $L=J\pm1$, even for pure $S$-state projectiles. In view of these difficulties, we select for our study the $^{58}$Ni$(d,\alpha)^{56}$Co$(7^+)$ at $E_d=22$ MeV, which has been analyzed already [7] with earlier VMC wave functions, and is a nonmixed transition therefore the most convenient case for our purpose. Since $^{58}$Ni is an $fp$-shell nucleus with the $f_{7/2}$ subshell full both of neutrons and protons, the stretched $7^+$ state can only be reached by a unique $L=6$, $J=7$ transition. The $L=8$ component would require both nucleon orbitals to be from the same higher shell, $g_{9/2}$ or above, which is energetically very unfavored.

The data for this reaction are shown in Fig. 5 from Ref. [7], along with our one-step predictions with an arbitrary normalization of the cross section $\sigma(\theta)$ by means of a chosen fixed target spectroscopic factor. We note first that variation of the spin-orbit strength for the bound state of the deuteron in the target allows us to obtain a better agreement for $A_y$ without significantly changing the tensor observables, as shown by the dash-dotted lines in the figure where this spin-orbit strength is reduced by 50%. Our main observation is that although with no $D$ state there are non-negligible tensor analyzing powers, there are important differences in $A_{yy}$ and in $A_{xx}$ arising from the projectile $D$ state. In both tensor

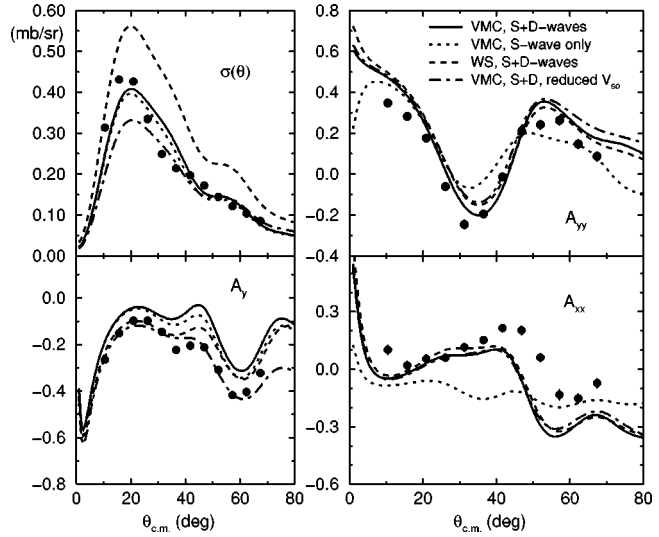


FIG. 5. $^{58}$Ni$(d,\alpha)^{56}$Co$(7^+)$ at $E_d=22$ MeV. The VMC curves use the revised results of Ref. [2], and the WS *D*-state curves use the same $\eta$ as the VMC model. The theoretical curves for $\sigma(\theta)$ are all arbitrarily normalized by the same factor.

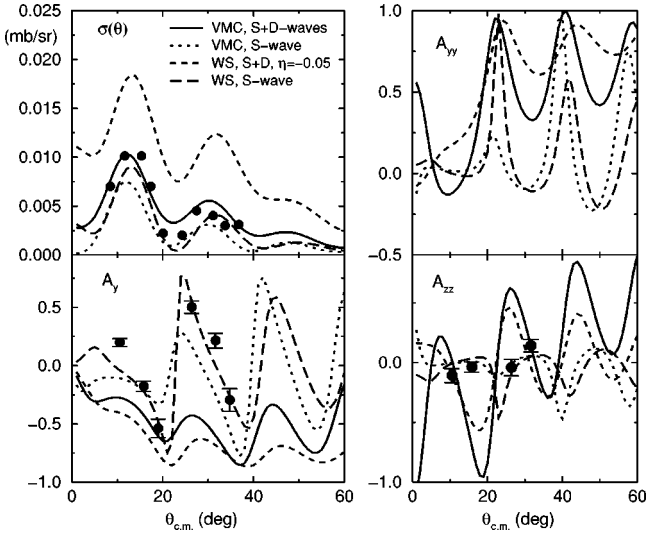


FIG. 6. $^{58}$Ni$(^6$Li$,d)^{62}$Zn$(0^+)$ at $E_{\rm Li}=34$ MeV. The VMC curves use the original results of Ref. [2], and the WS *D*-state curves use the same $\eta$ as the VMC model.

observables, the VMC and WS form factors generate quite similar curves, and the prediction is very close to the data in $A_{yy}$, particularly between 20° and 60°. Including the *D* state improves undoubtedly the agreement with the data in $A_{xx}$ at small angles, but the description is poor at larger angles. It is interesting to compare our results with those obtained by Crosson *et al.* [7], where they obtained for the case of $A_{xx}$ an agreement with the data over a wider angular region. They used two realistic vertex form factors arising from wave functions with stronger *D*-state components, associated with a $D_2=-0.16$ fm$^2$ and $D_2=-0.24$ fm$^2$. The data that allowed them to distinguish between those two descriptions clearly favored the less strong *D* component. In the more recent VMC vertex function we are now using, the *D* state is reduced even further. We can therefore conclude that, in spite of some dependence on the interior of the wave function that should encourage the use of realistic form factors for this type of analysis, the *D*-state amplitudes in the VMC models seem to be again underestimated.

Finally, we consider the more complicated $(d,^6$Li) transfer reaction. Unlike the *D*-state component in the overlaps of 1*s*-shell nuclei which are generated solely by tensor forces, the *D* state in the $d+\alpha$ configuration of $^6$Li can also result from its *p*-shell structure. The fraction of this *D* state has been the subject of considerable theoretical and experimental investigation. There have been many three-body models of $^6$Li constructed in the literature [12–14], and in spite of the excellent agreement with several properties of $^6$Li that these models achieve, none of them have been able to reproduce the spectroscopic quadrupole moment of the $^6$Li ground state of $-0.083\pm0.008$ $e$ fm$^2$ [15]. They all predict a *positive* quadrupole moment and, unavoidably, a positive $\eta$ value. It is clear that there must be in reality some cancellation of the intrinsic deuteron moment with the *D* state of relative motion, or some hitherto unexpected contributions from degrees of freedom outside the $\alpha+n+p$ model space. We therefore are pleased to see negative quadrupole moments from ''no core'' shell models [16] (though with rather small matter radius of $^6$Li), and also from the new VMC results of Refs. [2,4]. Unfortunately, the VMC calculations obtain the quadrupole moment of the $^6$Li ground state as $-0.8\pm0.2$ $e$ fm$^2$ [2], rather *too* negative compared with the observed value. It is important to emphasize that although less interesting for the study of the tensor force, $\eta$ in $^6$Li is a very interesting observable, which enables us to understand the low-energy dynamics in $^6$Li, and to test $\alpha+d$ and $\alpha+n+p$ cluster models as well as six-body variational calculations.

From the experimental point of view, several determinations based on the analysis of different reactions gave quite different results. The analysis of elastic scattering of $^6$Li on $^{58}$Ni points to negative values for $\eta$, namely $-0.014$ from the analysis at 18.1 MeV [18] and at 70.5 MeV [17], and about half that value in a later reanalysis [19] of the same reaction. Data on $^6$Li$(d,\alpha)^4$He [20] also indicated a negative value of the $\eta$ parameter. By contrast, in a forward dispersion relation analysis of $d$-$\alpha$ scattering, the value found for $\eta$ was positive [21], as in the analysis of the breakup of the $^6$Li at 4.5 GeV [22]. Very recently, in the analysis of a $(^6$Li$,d)$ transfer reaction on $^{58}$Ni target 34 MeV [9], the parameter seems to be consistent with zero. This last value is the one quoted in Table I as an experimental determination. In view of these discrepancies, it is therefore valuable to examine a further consequence of the *D* states in the $d+\alpha$ motion, by looking at the analyzing powers in a $(d,^6$Li) transfer reaction.

We will consider for our study the $^{58}$Ni$(^6$Li$,d)^{62}$Zn$(0^+)$ reaction that has been measured very recently at $E_{\rm Li}=34$ MeV [8,9], where there are only pure *L* transfers allowed from *S*-state overlaps. This means that we regain the scaling relation between the tensor analyzing powers and the $D/S$-state ratios $\eta$ of the projectile, and it should be possible to measure even very small $\eta$ values. The results for this reaction are shown in Fig. 6 from Refs. [23] and [8,9]. The dotted curve shows the VMC prediction from Ref. [2] for just the *S* state, while the solid curve shows the effect of adding the *D* state. We see that in fact the dotted curve is

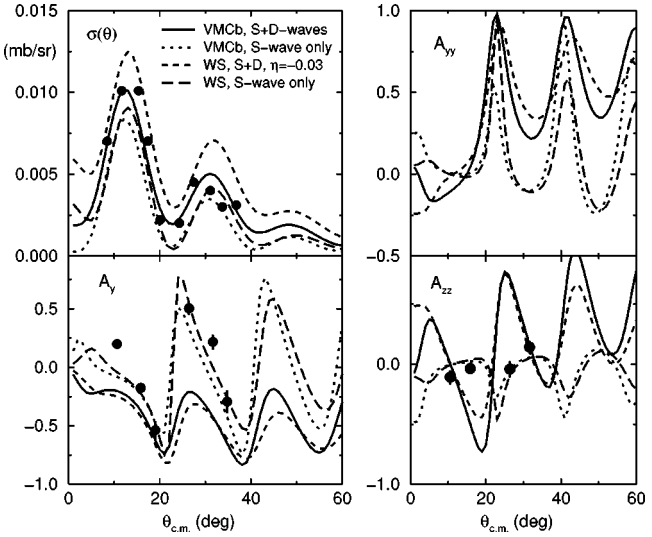


FIG. 7. $^{58}$Ni($^{6}$Li,$d$)$^{62}$Zn($0^{+}$) at $E_{\mathrm{Li}}=34$ MeV. The VMC curves use the revised results of Ref. [4], and the WS $D$-state curves use the $\eta$ value of the VMC model.

close to the data, but the $D$ state effectively destroys the fit, even for the vector analyzing power $A_y$. The experiment is therefore pointing to a best-fit $\eta$ value much smaller than that of the VMC model. The $S+D$ WS curves in Fig. 6 (short dashes) show that the $D$ state effects derived from a conventional WS geometry when normalized to the VMC $\eta$ value, give rather different results from the VMC solid curve, even for the cross section $\sigma(\theta)$. We see large differences between VMC and WS wave functions, both for just $S$ waves, and for $S+D$ waves. The effects of the WS $D$ state normalized to $\eta=-0.05$ are more than those the VMC $D$ state. These differences all indicate that the geometry of the $D$-state vertex function in the VMC model from Ref. [2] is rather different from that of a conventional WS binding potential. The WS model with $\eta=0$ is closest to the data, and the analysis of Ref. [9] shows that the best fit value is the very small $\eta=+0.0003(9)$.

More recently, a new VMC result has become available [4] that appears to be closer to convergence. This has only about half the $D$-state amplitudes of the model of Ref. [2], and the tensor analyzing powers obtained with this new model are shown in Fig. 7. The WS curves in this figure use the VMC value $\eta=-0.03$, and we now see that the WS and VMC results are rather similar. This indicates that the new VMC model has a more regular geometry in its $D$-state component; but unfortunately these $D$-state amplitudes are still too large compared with experiments.

From all the comparisons of transfer predictions with the experiments shown here that come close to the data, we conclude that for $(d,t)$ and $(d,{}^{3}\mathrm{He})$ and $(d,\alpha)$ the $D$-state component of the overlaps from the VMC models is somewhat underestimated. In the case $^{6}$Li VMC models produce an overlap with a $D$-state component many times larger than appropriate to fit the experimental analyzing powers. This enhancement of the $D$-state component is certainly one of the reasons for the too strong quadrupole moment $Q$ of $^{6}$Li that these models predict. Since the correlation between $\eta$ and $Q$ in this case may be not be simple, quadrupole moment and electron form factor measurements are needed together with the nuclear transfer experiments discussed here.

## ACKNOWLEDGMENTS

We are grateful for many discussions with F.D. Santos, with our experimental colleagues at UNC/TUNL, in particular Ed Ludwig and Kevin Veal. This work was supported in part by the Portuguese FCT under Contract No. Praxis/2/2.1/FIS/223/94 and EPSRC under Grant Nos. GR/L94574 and GR/J95867.

[1] A. M. Eiró and F. D. Santos, J. Phys. G **16**, 1139 (1990).
[2] J. L. Forest, V. R. Pandharipande, S. C. Pieper, R. B. Wiringa, R. Schiavilla, and A. Arriaga, Phys. Rev. C **54**, 646 (1996).
[3] R. B. Wiringa, V. G. J. Stoks, and R. Schiavilla, Phys. Rev. C **51**, 38 (1995).
[4] R. B. Wiringa (private communication).
[5] B. Kowslowka, Z. Ayer, R. K. Das, H. J. Karwowski, and E. J. Ludwig, Phys. Rev. C **50**, 2695 (1994).
[6] Z. Ayer, H. J. Karwowski, B. Kowslowka, and E. J. Ludwig, Phys. Rev. C **52**, 2851 (1995).
[7] E. R. Crosson *et al.*, Phys. Rev. C **45**, R492 (1992); **47**, 2690 (1993); **48**, 1770 (1993).
[8] K. D. Veal *et al.*, Bull. Am. Phys. Soc. **40**, 2064 (1995).
[9] K. D. Veal *et al.*, Phys. Rev. Lett. **81**, 1187 (1998).
[10] A. M. Eiró and F. D. Santos, Nucl. Phys. **A234**, 301 (1974).
[11] I. J. Thompson, Comput. Phys. Rep. **7**, 167 (1988).
[12] D. R. Lehman, Colloq. Phys. **51**, C6-47 (1990), and references therein.
[13] N. W. Schellingerhout, L. P. Kok, S. A. Coon, and R. M. Adam, Phys. Rev. C **48**, 2714 (1993); **52**, 439 (1995).
[14] V. I. Kukulin, V. N. Pomerantsev, Kh. D. Razikov, V. T. Voronchev, and G. G. Ryzhikh, Nucl. Phys. **A586**, 151 (1995).
[15] D. Sundholm *et al.*, Chem. Phys. Lett. **112**, 1 (1984).
[16] P. Navrátil and B. R. Barrett, Phys. Rev. C **54**, 2986 (1996).
[17] P. R. Dee, C. O. Blyth, H. D. Choi, N. M. Clarke, S. J. Hall, O. Karban, I. Martel-Bravo, and S. Roman, Phys. Rev. C **51**, 1356 (1995).
[18] H. Nishioka, J. A. Tostevin, R. C. Johnson, and K.-I. Kubo, Nucl. Phys. **A415**, 230 (1984).
[19] K. Rusek, N. M. Clarke, G. Tungate, and R. P. Ward, Phys. Rev. C **52**, 2614 (1995).
[20] F. D. Santos, I. J. Thompson, and A. M. Eiró, Colloq. Phys. **51**, C6-443 (1990).
[21] M. P. Bornand, G. R. Plattner, R. D. Viollier, and K. Alder, Nucl. Phys. **A294**, 492 (1978).
[22] V. Punjabi *et al.*, Phys. Rev. C **46**, 984 (1992).
[23] R. R. Betts *et al.*, Phys. Lett. **76B**, 47 (1978).